



Fatigue strength modelling of high-performing welded joints

Heikki Remes^{a,*}, Pasquale Gallo^a, Jasmin Jelovica^b, Jani Romanoff^a, Pauli Lehto^a



^a Aalto University, School of Engineering, Department of Mechanical Engineering, P.O. BOX 14100, FIN-00076 Aalto, Finland

^b The University of British Columbia, Faculty of Applied Science, Department of Mechanical Engineering, 6250 Applied Science Ln #2054, Vancouver, BC V6T 1Z4, Canada

ARTICLE INFO

Keywords:

Fatigue strength
Welded joint
Strain-based approach
Notch stress approach
Strain energy density

ABSTRACT

This paper investigates the fatigue strength modelling of high-performing welded steel joints. The work considers the strain-based, notch stress, averaged strain energy density approaches, and linear elastic fracture mechanics. A comparison of the methods with experimental data shows that the predictions vary significantly for different modelling assumptions. Only the microstructure-sensitive strain-based approach can predict the fatigue life of various weld geometries and plate thicknesses. The explicit modelling of the localised plasticity using the microstructure-dependent representative volume element is required for accurate prediction of the short crack initiation and growth periods, which dominate the fatigue life modelling of high-performing welds.

1. Introduction

The first concept of the fatigue strength modelling of welded structures was defined by the early works of Wöhler and Basquin; see [1,2]. The established Wöhler (or S-N) curve concept predicts the fatigue life by comparing the reference stress S to the experimentally defined fatigue life N . Since the Wöhler curve, several other modelling methods have been introduced; see e.g. [3]. In terms of modelling, the most important concepts are the Coffin-Manson relationship and Paris' law; see [4–7]. The first concept links cyclic elastic and plastic strain amplitudes to material fatigue life, i.e. macro crack initiation, N_i , while the latter allows the modelling of the crack growth period, N_p . In recent decades, significant effort has been made in terms of multi-scale modelling and accurate consideration of crystal plasticity; see e.g. [8,9]. The microstructure-sensitive plasticity models aim to develop the original Coffin-Manson relationship further in order to explicitly consider the effects of the microstructure on fatigue damage accumulation at the grain level. Paris' law has also been extended, e.g. for different loading histories. Similarly, the applicability of the Wöhler curve concept has been extended by the development of different reference stress definitions such as structural and notch stress; see e.g. [10]. However, limited effort has been made to develop the S-N curve concept further to cover both crack initiation and growth explicitly in the same model. In the last decade, this kind of continuum-based fatigue strength modelling has received interest thanks to the need for new high-performing lightweight solutions and improved sustainability of the structures used in transportation, mechanical, and civil engineering [11].

Increased load-carrying capacity and weight reduction of large structures such as ships is possible if thinner plates, high-strength steels, and efficient structural topologies are utilised. The main limiting design factor is the fatigue strength assessment of these complex welded structures [11]. The key modelling challenges are the considerations of (1) welding-induced distortion and weld bead shape (i.e. macro-geometrical features), (2) weld notch shape and imperfections (i.e. micro-geometrical features), and (3) material effects; see e.g. [11]. For example, in thin plate structures the welding-induced distortions can result in significant secondary bending stress in fatigue-critical welds. Furthermore, unfavourable weld notch shapes and weld imperfections such as undercuts increase the stress concentration and may significantly reduce fatigue strength [12–14]. In thin-walled and high-strength steel structures, the management of weld imperfections is becoming increasingly important; see e.g. [15–18]. These challenges can be solved by using a well-controlled manufacturing process, and excellent fatigue strength can be obtained for welded joints and full-scale structures [19–25]. As shown in Fig. 1, the current fatigue design curve (FAT100) is significantly exceeded by a high-performing welded joint (FAT > 200 MPa). However, the utilisation of this fatigue strength potential is not possible since existing fatigue strength modelling methods have their limitations.

The key challenge in the fatigue strength modelling of large welded structures is that the detailed geometry and material modelling of fatigue critical structural details is time-consuming. A large structure like a cruise ship can include several hundred kilometres of weld seams, both in the hull girder and in the superstructure. As the hull girder

* Corresponding author.

E-mail address: heikki.remes@aalto.fi (H. Remes).

Nomenclature		β	Notch opening angle
<i>Symbols</i>		ε_f	Fatigue ductility coefficient
ΔW	Average strain energy density range	ν	Poisson's ratio
ΔW_a	Average strain energy density range for 2 million load cycle	θ	Weld flank angle
ΔK_{th}	Threshold value of stress intensity factor	ρ	Notch root radius
$\Delta \sigma$	Stress range	σ	Stress
A	Area of cross-section	σ_f	Fatigue strength coefficient
a	Crack length	σ_y	Yield strength
b	Fatigue strength exponent	<i>Subscripts</i>	
C	Paris law constant	i, p, f	Initiation, propagation, failure
c	Fatigue ductility exponent	eff	Effective
D	Notch depth	t, r	Toe, root
d	Averaged grain size	n, m	Crack growth step indexes
$d_{99\%}$	Grain size at a 99% probability level	cri	Critical
d_v	Volume-weighted average grain size	nom	Nominal
E	Young's modulus	hs	Structural hot-spot
E_T	Tangent modulus	<i>Abbreviation</i>	
F	Force, safety factor for survival probability level of 97.7%	BS	British standard
h	Weld height	CGR	Crack growth rate
K	Strain-hardening coefficient	ENS	Effective notch stress approach with a fictitious rounding of 1 mm
K_I	Stress intensity factor	FAT	Fatigue class, characteristic fatigue strength at 2 million load cycle
k	Inverse slope of ΔW -life curve	FEA	Finite element analysis
k_f	Fatigue notch factor	HAZ	Heat affected zone
k_m	Stress magnification factor	HM	Martens Hardness
m	Inverse slope of S-N curve	HV	Vickers Hardness
N	Fatigue life, number of cycles	IIW	International Institute of Welding
n	Paris law slope coefficient, strain-hardening exponent	LEFM	Linear elastic fracture mechanics
P	Probability for failure	PM	Parent material
P_{SWT}	Fatigue damage parameter according to Smith, Watson and Topper	R _{ref}	Effective notch stress approach with a fictitious rounding of 0.05 mm
R	Load ratio	RVE	Representative volume element
R_o	Control volume radius	SCG	Strain-based crack growth approach
s	Distance from crack tip perpendicular to the maximum principal stress direction	SED	Strain energy density approach
S	Reference stress	WM	Weld metal
t	Plate thickness	PF	Primary ferrite
T_σ	Scatter range index, fatigue strength ratio of 10% and 90% failure probability levels	P	Pearlite
w	Weld width	AF	Acicular ferrite
ΔK_I	Range of stress intensity factor		

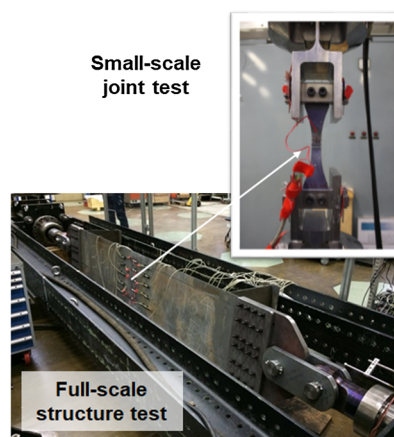
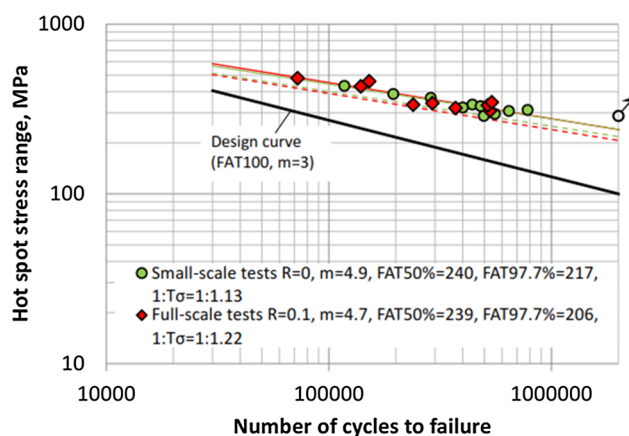


Fig. 1. Fatigue strength of a high-performing laser-hybrid welded butt joint in a thin plate structure. Both small- and full-scale experiments are included [11].

deforms in waves, fatigue failure can initiate at multiple locations simultaneously. In design, the structural stress approach is commonly applied to determine the highly stressed locations prone to fatigue failure. This method has an excellent balance between computational cost and accuracy; see e.g. [21,23]. In the structural stress approach, the reference stress for fatigue assessment is defined using a simplified finite element model of the real structure. The fatigue life is predicted using an S-N curve derived from the experiments on representative small-scale specimens. The structural stress approach considers the macro-geometrical effects but neglects explicit modelling of the stress concentration induced by weld notches. Thus, the weld notch effect is considered implicitly through the reference S-N curve. This approach, based on the Wöhler curve concept, is applicable if the geometry of the welded joint is similar to the reference data used for the determination of the S-N curve. Therefore, while the S-N curves typically contain a broad variation of weld geometries, a well-controlled manufacturing process can produce welded joints with favourable geometries that represent only the high-strength portion of the statistical sample; see [19,24], and [25]. This difference causes undesirable conservativeness in fatigue strength modelling, and thus new structural stress S-N curves are needed for high-performing welds and structures. High-performing weld is result of high-precision manufacturing and better quality control, leading to superior fatigue strength. Thus, fatigue design of these welds is related to manufacturing technology applied and resulted geometrical properties. To define weld geometrical property-based acceptance criteria for different fatigue classes, the development of quality-based fatigue design rules has been initiated; see e.g. [26]. This development requires systematic experimental work and numerical analyses with local fatigue approaches, such as the notch stress approach, that models the weld geometry explicitly; [21]. In comparison to the original Wöhler curve concept, these local fatigue approaches utilise the local stress or strain calculated within a control volume, instead of nominal stress.

When discussing the fatigue strength modelling of welds, it is important to distinguish a normal, i.e. low-performing, weld and a high-performing weld. A normal weld can incorporate crack-like defects such as sharp undercuts and it is thus commonly assumed that the crack propagation life N_p dominates the total fatigue life. Consequently, the initiation life N_i is assumed to be negligible. This assumption is not valid for a high-performing weld with favourable notch geometry and a small micro-geometrical effect. A longer initiation time can lead to a significant difference in the fatigue strength and life in comparison to a normal weld; see e.g. [18,25–31]. Accurate modelling of this difference might be a challenge for the existing stress-based local approaches, which give a quick fatigue life prediction by using the local stress or strain value together with the S-N curve for the total fatigue life [21]. In the case of high-performing welds, the local approaches can lead to inaccuracies in fatigue life predictions since these approaches are preferable to modelling crack initiation close to endurance limit; a localised control volume and linear elastic material model with small-scale yielding assumption are used. Consequently, the suitability of different

local approaches and modelling assumptions for the prediction of the fatigue strength and life of high-performing welds should be investigated further.

In this paper, the influence of variations in the weld geometry on fatigue strength modelling is investigated. The research shown in this paper is a continuation of the work initiated in [22]. This paper extends the previous work by covering several different local approaches and includes the influence of plate thickness together with material microstructural effects. A workflow of the paper is the following. In Section 2, the requirements for geometry and material modelling of high-performing welds are discussed. Then, the modelling requirements are reflected to the fundamental assumptions used in local approaches. To cover different modelling assumptions, this study includes microstructure-sensitive strain-based crack growth approach, crack propagation approach based on linear elastic fracture mechanics, averaged strain energy density approach, and effective notch stress approach; see Fig. 2. Section 3 explains details of numerical simulations for fatigue life comparisons. The comparisons is done using the case study, which includes one normal and two high-performing butt-weld geometries. The results of numerical analyses are shown in terms of structural stress and they are compared with fatigue test results for welds with different quality i.e. performance levels. The study includes both thick and thin plates in order to reveal the effect of the thickness-dependent stress gradient on the fatigue strength modelling. In Section 4, the comparison of the methods is presented. Furthermore, the influence of the weld geometrical shape on fatigue crack initiation and growth are discussed. The paper ends with a holistic discussion and conclusions in Sections 5 and 6, respectively.

2. Fatigue strength modelling approaches

2.1. Geometry and material modelling of high-performing welds

Welded joints can be divided, on the basis of their fatigue strength, into normal and high-performing welds. However, providing an accurate definition in terms of macro- and micro-geometrical features is a challenge. Indeed, the definition that currently exists covers only normal welds. The normal welds may include weld imperfections as specified in guidelines and different standards; see e.g. [32,33]. Because of crack-like imperfections, e.g. a 0.1–0.2-mm initial crack, their fatigue strength is mainly dependent on macro-geometrical features such as weld bead shape and welding-induced angular misalignment. For this study, the high-performing welds are defined physically as a beneficial combination of the micro-geometrical features, i.e. weld notch geometry and material properties, which together yield reduced plasticity and crack driving force because of the absence of crack-like imperfections. This beneficial combination is seen as a superior fatigue strength in comparison to normal welds as illustrated in Fig. 1. Mathematically, the definition is based on the macro crack initiation and propagation time, i.e. $N_f = N_i + N_p$. For a high-performing weld, the macro crack initiation life also contributes significantly to the total fatigue life in the

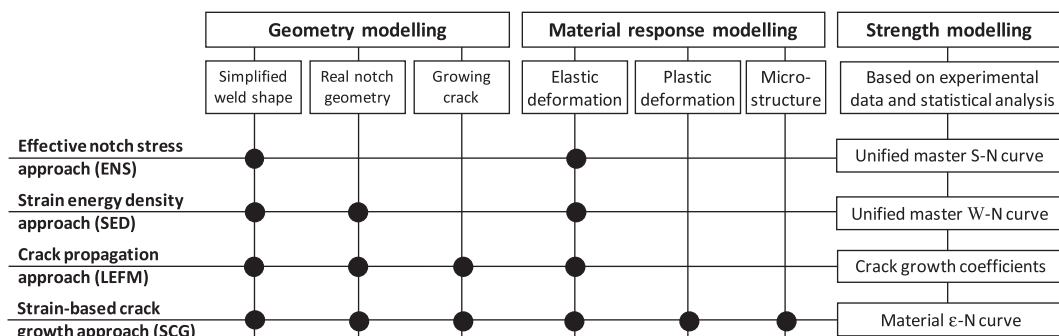


Fig. 2. The considered local approaches and their modelling competences.

medium-cycle range ($N_f = 10^4\text{-}10^6$), i.e. $N_i > 0.5 \cdot N_f$. In order to capture the crack initiation period, robust modelling of the influence of weld notch geometry and material stress-strain behaviour on fatigue damage accumulation is crucial. In addition to the weld's macro geometry, micro-geometrical features such as weld notch shape need to be characterised since they affect the stresses and strains at the location of fatigue damage. Fig. 3 proposes a simplified geometry modelling approach for high-performing welds in which the depth and radius of undercut are able to describe the micro-geometrical features for varied weld sizes and bead shapes. Since the crack initiation time is significant, the modelling of both the notch-induced stress gradient and material effects is equally important. Furthermore, when continuum-based modelling, such as the Coffin-Manson relationship, is considered, the material has an influence on both the response (dislocation-induced plasticity) and fatigue strength (formation of sub-grain boundaries, crack nucleation and crack formation). Thus, the material modelling affects the crack driving force, as the plastic response and fatigue damage area evolve after a crack has been initiated from the weld notch. Consequently, the modelling of a crack driving force should be unified to consider the internal and external loading, plastic deformation behaviour, and the microstructure-dependent representative volume element where the fatigue damage occurs. To illustrate the influence of these key modelling factors on fatigue strength and life prediction, we first introduce a model that covers all these aspects explicitly. Then the results are compared to various local approaches that can only include these aspects partially, either implicitly or explicitly.

2.2. Microstructure-sensitive strain-based crack growth modelling

A robust fatigue approach should be able to explicitly model (1) the initial weld geometry and its changes during crack growth, (2) the elastic-plastic behaviour of the material, and (3) the influence of the microstructure of the material on accumulated fatigue damage and, consequently, the crack growth. The recently published Strain-based Crack Growth (SCG) approach includes these modelling aspects while still being suitable for welded joints; see [34,35]. In this approach, the initiation and growth of the fatigue crack are modelled as an accumulative fatigue damage process within a Representative Volume Element (RVE). The definition of RVE combines the property- and microstructure-based statistical equivalence in order to be suitable for different materials and materials zones. The RVE size is defined as the size that shows convergence between averaged material hardness i.e. local plastic deformation and a characteristic value of grain size statistics. Based on the experimental and statistical study in [36–38], the RVE size is defined as grain size at a probability level of 99%, $d_{99\%}$. This shows excellent convergence for different welded steels material and material zones as shown in Fig. 4. This definition for RVE is in line with the Hall-Petch relation since the weakest material point (i.e. lowest strength) can be related to the largest grain size; see [39,40]. Thus, the size of this microstructure-dependent RVE depends on the material microstructure e.g. parent material property and applied welding and manufacturing process. For instance in the case of low

strength structural steel, the RVE size of $27 \mu\text{m}$ for the parent material, $56 \mu\text{m}$ for HAZ of submerged arc weld, and $10 \mu\text{m}$ for HAZ of laser-hybrid weld due to differences in grain size dispersion [34].

Using the microstructure-dependent RVE as a calculation unit, the fatigue crack initiation and growth is modelled as repeated fatigue damage process. Hence, the analysis uses the measured initial geometry of the notch as a starting point. After the failure of the initial RVE, the crack is propagated through successive RVEs until the final fracture is reached. Thus, the fatigue crack initiation, short crack growth, and long propagation behaviour are all considered as a continuous process in the same model, as shown in Fig. 5. In Fig. 5 the results are plotted as a function of effective crack length, where RVE size ($d_{99\%} = 0.01 \text{ mm}$) is considered as an initial crack size. During the crack growth, the stress concentration and stress gradient increase, affecting the amount of plasticity in the RVE. For short cracks (Period A in Fig. 5), the size of the plastic zone is smaller than the size of the RVE and the crack tip behaviour is mainly linear elastic, while for macro cracks (Period B in Fig. 5) the size of the plastic zone is larger than that of the RVE and crack tip blunting is visible. For long cracks (Period D in Fig. 5), the crack tip constrain effect is suddenly lost as a result of high plasticity (Point C) and the radius of the blunted crack tip is large in comparison to the size of the RVE. These changes in the plasticity of the RVE have an influence on the cyclic stresses and strains, resulting in different growth rates of fatigue damage (e.g. an increased rate of the Smith Watson and Topper fatigue damage parameter P_{SWT}). It is worth mentioning that the crack growth rate (CGR) obtained by an SCG approach, calculated through a microstructure-sensitive strain-based approach, has shown very good agreement with experimental CGR measurements [34].

In SCG analysis, the fatigue-effective stresses and strains are defined as average values over the RVE since latter defines the material volume in which continuum-based modelling can be used to describe fatigue damage (i.e. the nucleation and coalescence of micro cracks) causing microscopic crack growth; see [34]. Thus, the fatigue effective stress is

$$\sigma_{eff} = \frac{1}{d_{99\%}} \cdot \int_0^{d_{99\%}} \sigma ds \quad (1)$$

where $d_{99\%}$ is the grain size at a probability level of 99% i.e. material characteristic length and σ is the maximum principal stress. Accordingly, the maximum principal stress distribution is averaged over distance $d_{99\%}$ in the direction of the coordination axis s , which starts from the notch tip and is perpendicular to the direction of the maximum principal stress; see [35]. The calculation of the stress distributions at the notch or in the crack area is carried out using the finite element method in order to have robust elastic-plasticity analysis. The minimum element size, defined on the basis of the microstructure of the material and result convergence, is at least ten times smaller than RVE size to model non-linear deformation shape of the RVE using linear 4-node elements. The non-linear material behaviour is described using the isotropic hardening rule and the von Mises yield criterion. In order to model the plastic deformation occurring during the first initial load cycle and followed material cyclic hardening or softening, separate

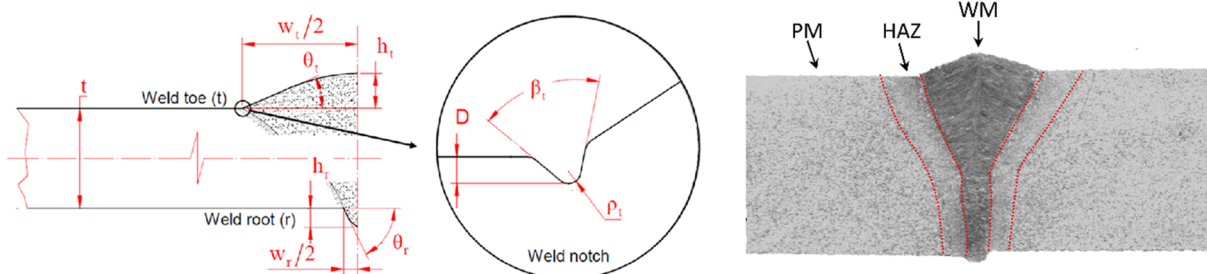


Fig. 3. Proposed geometry and material modelling of a high-performing weld, including the macro geometry (weld width w , weld height h , weld flank angle θ), micro geometry at the weld notch (notch depth D , notch opening angle β , and notch root radius ρ), and different material zones (parent material PM, heat-affected zone HAZ, weld metal WM), modified from [35].

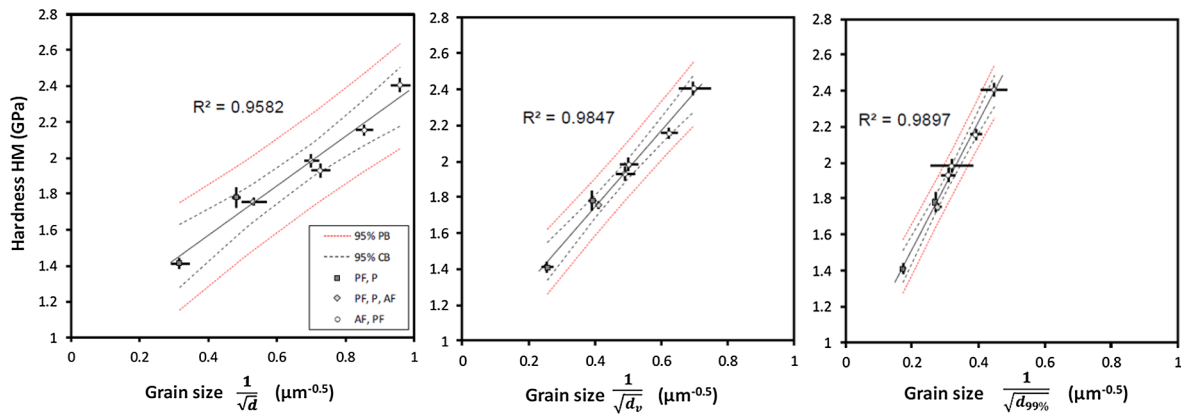


Fig. 4. Martens Hardness HM of ferritic parent materials metal (PF, P) and weld metals (PF, P, AF; AF, PF) as a function of different grain size parameters: average grain size d , volume-weighted average grain size d_v , large grain size at a 99% probability level $d_{99\%}$, modified from [36,37].

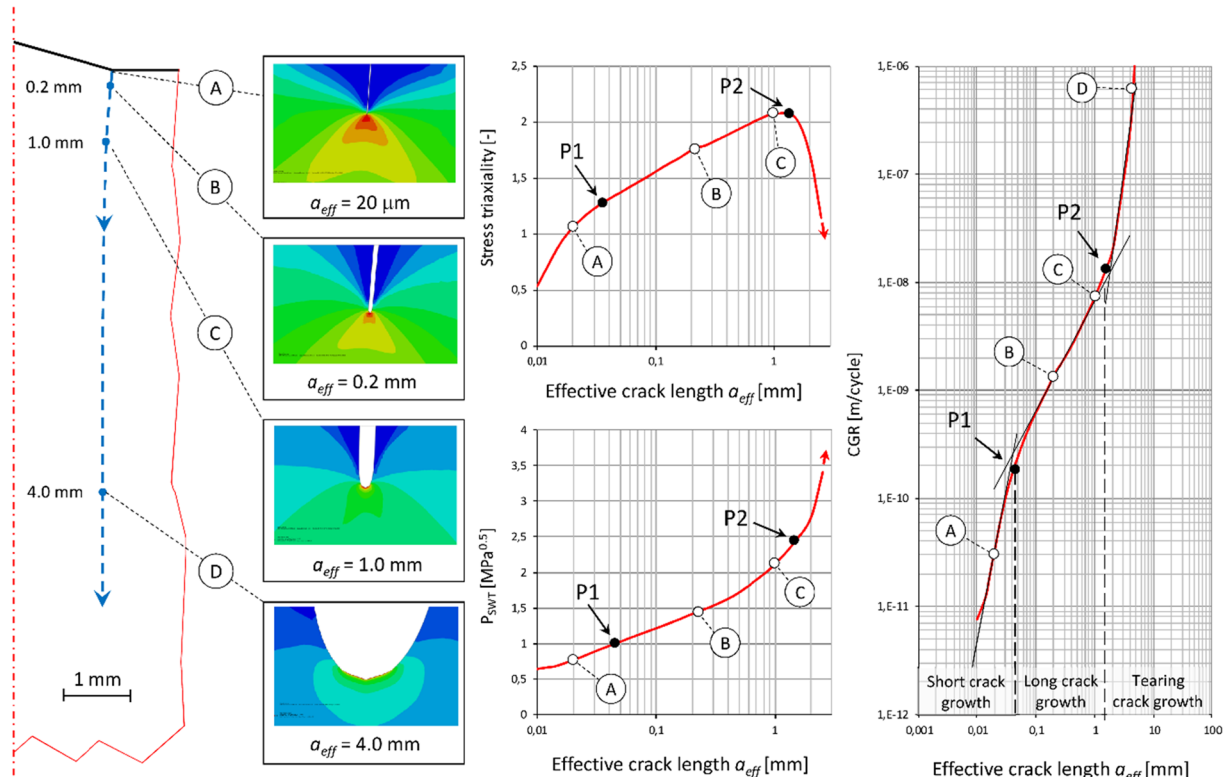


Fig. 5. Example of SCG analysis for crack initiation and propagation based on a strain-based continuum damage model. The development of the calculated stress triaxiality, damage parameter P_{SWT} , and crack growth rate as a function of effective crack length are shown, modified from [35].

stress-strain curves are applied for initial monotonic and following cyclic loading for each crack growth step. Consequently, the FE analysis includes two steps within which the monotonic stress-strain curve is applied to calculate the maximum stress σ_{max} . Then the strain amplitude ϵ_a is calculated using the cyclic stress-strain curves. Alternatively, combined isotropic and kinematic hardening models can be used considering both monotonic and cyclic material behaviour with one material model; see [41].

The fatigue life, i.e. the load cycles corresponding to crack initiation N_{in} and to each growth step n , is calculated on the basis of the fatigue-effective stresses $\sigma_{max,eff}$ and strains $\epsilon_{a,eff}$ by using the fatigue damage parameter P_{SWT} [42] and the Coffin-Manson relationship (see [4,5]):

$$\sigma_{max,eff} \cdot \epsilon_{a,eff} = \left[\frac{\sigma_f'^2}{E} \cdot (2 \cdot N_{in})^{2-b} + \sigma_f' \cdot \epsilon_f' \cdot (2 \cdot N_{in})^{b+c} \right] \quad (2)$$

where the parameters σ_f' , ϵ_f' , b , and c are the fatigue strength coefficients [34]. The hardness-based estimation for the fatigue strength coefficients [43] is used in this case.

The total fatigue life for the final fracture N_f is the sum of the load cycles covering initiation ($n = 0$) and all the growth steps ($n = 1 \dots m$). Furthermore, on the basis of the number of load cycles N_{in} at the step n , the crack growth rate CGR can be calculated at a certain crack length from:

$$CGR(a_{eff}) = \frac{d_{99\%}}{N_{in}(a_{eff})} \quad (3)$$

This crack growth rate CGR is always related to a certain crack length, as shown in Fig. 5, and thus it enables a comparison to be made between the SCG results and the results based on the fracture mechanics approach using the stress intensity factor K_I . In the calculation of K_I for the SCG analysis results, the effective crack length ($a_{eff} = D + a + d_{99\%}$)

is used to cover whole damage process from zero crack length until final fracture. Furthermore, the crack-like undercut with depth D is considered since it acts as an additional initial crack size to actual crack size a in the crack propagation analysis shown in Section 2.3.

2.3. Linear elastic crack propagation modelling

When the weld geometry includes sharp undercuts, the following simplifications are possible. First, the initial geometry can be modelled as a crack, resulting in the elastic stress distribution ahead of the crack tip, the shape of which remains the same during crack growth, i.e. the fatigue life. Second, because of the high stress concentration at the crack tip and small-scale yielding in the infinitesimal volume, a linear elastic material model can be used. Then, because of the similitude in stress distribution between cracks of different sizes, the influence of the microstructure of the material on the accumulated fatigue damage can be described with simplified material parameters instead of the explicit modelling of plasticity.

A well-known model that applies these assumptions is Paris' law [7], which uses linear elastic fracture mechanics (LEFM) to predict number of cycles in stable crack propagation domain. In LEFM, the material is assumed to be elastic and the damage is assumed to occur in an elliptical notch with an infinite aspect ratio. Thus, the notch geometry is idealised as a crack and the crack initiation period is neglected. The stress field solution around the crack tip is described by the Williams solutions from elasticity theory [44]. Then the explicit consideration of load-redistribution resulting from plasticity is neglected and this effect is obtained implicitly through the material parameters. On the basis of the Williams solutions, the stress intensity factor for a crack tip, K_I , can be formulated, and the fatigue crack propagation time N_p to reach the critical crack length a_{cri} is calculated utilising Paris' law:

$$N_p = \int_{a_i}^{a_{cri}} \frac{1}{C \cdot \Delta K_I^n} da \quad (4)$$

where C is the crack growth coefficient and n the slope of the growth rate curve. Eq. (4) is solved using the numerical integration and piecewise cubic hermite interpolation. The crack growth increment of 0.001 mm is used to ensure convergence of the results.

2.4. Reference S-N curve concept

Assuming that the weld's micro-geometrical features, material

behaviour, and crack driving force are similar for different welds, the concept of similitude can be applied to a wider scope. With these assumptions, the modelling of fatigue strength can be performed with one independent variable and one dimensionless parameter to transfer generic information (e.g. fatigue damage behaviour and process) between different welds. Several local fatigue approaches utilise this concept, and they are referred to as reference stress or S-N curve approaches. Two well-known spin-off approaches from the original Wöhler curve concept are the effective notch stress approach (ENS) and averaged strain energy density approach (SED). The former uses the reference stress obtained at the weld notch with a fictitious rounding radius. The latter uses the averaged strain energy density within a control volume located around the actual notch geometry. Similarly to several other local approaches, ENS and averaged SED define their reference stress (or energy) on the basis of the crack initiation phase, without explicit consideration of the plasticity of material and load redistribution resulting from crack growth. The dimensionless parameter for transferring generic information is obtained from the S-N curve, which links the reference stress or strain energy to the total fatigue life. Both ENS and SED are efficient engineering approaches for the prediction of fatigue strength. However, their general use might be limited to some specific application range since they do not explicitly model crack propagation. Since the ENS and SED analyses are purely based on the initial geometry, they do not consider explicitly the changes in local stresses and strains due to crack growth.

2.4.1. Strain energy density approach

The averaged strain energy density (SED) approach averages energy within a control volume located around the actual weld notch geometry [45–47]. The strain energy density is defined within a given control volume, which, in the case of two-dimensional problems, is a circle or a circular sector with the radius R_0 ; see Fig. 6. A unified averaged SED curve (ΔW -life curve) with a fixed control volume is used to determine the fatigue life [48,49]. The averaged SED value is evaluated using FE simulations under linear elastic conditions. The SED value ΔW at the selected nominal stress range is obtained, and the corresponding fatigue life is calculated using the ΔW -life curve:

$$N_f = (\Delta W_a / \Delta W)^k \cdot 2 \cdot 10^6 \quad (5)$$

where ΔW_a is the average strain energy density for two million load cycles.

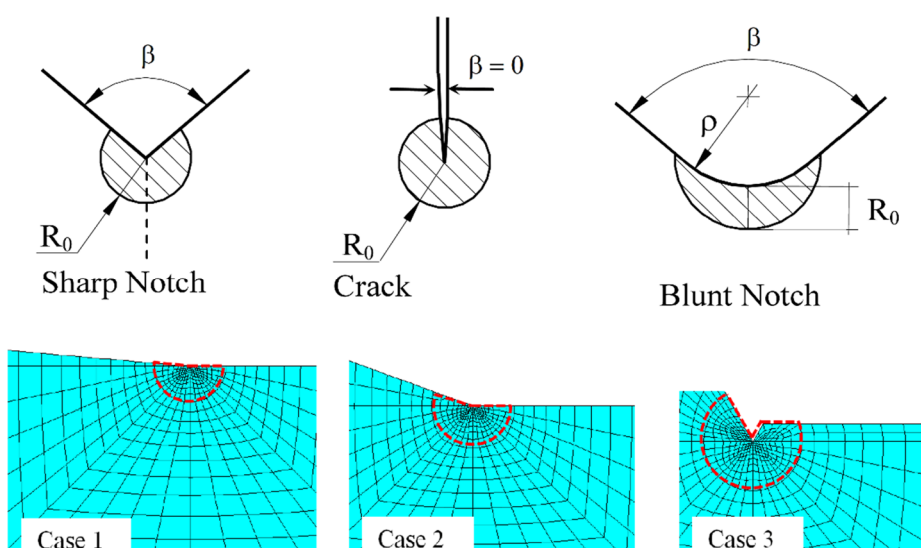


Fig. 6. Control volume (area) around a sharp V-notch, crack, and blunt notches (top) and actual weld geometry together with the control volume R_0 with a radius of 0.28 mm for Case 1, Case 2, and Case 3 (below).

2.4.2. Effective notch stress approach

The effective notch stress approach (ENS) uses a fictitious rounding radius to determine a reference stress [21]. Thus, the real notch geometry is replaced by the fictitious rounding to acquire an efficient analysis methodology for engineering purposes. Usually, a radius of 1 mm is used for modelling weld notches and it considers a material support effect as shown in Fig. 7; see also [10,50]. Since the 1-mm fictitious radius can affect the stiffness of welded joints for plate thicknesses less than 5 mm [32], the notch stress approach with a fictitious rounding of 0.05 mm has been introduced, together with a redefinition of the master S-N curve. This approach is marked here as $R_{ref} = 0.05$ mm, [53]. For both methods, ENS and $R_{ref} = 0.05$ mm, the notch stress is defined by the fine mesh FE analysis and mesh size independent strength value derived from the experiments; see [32,50].

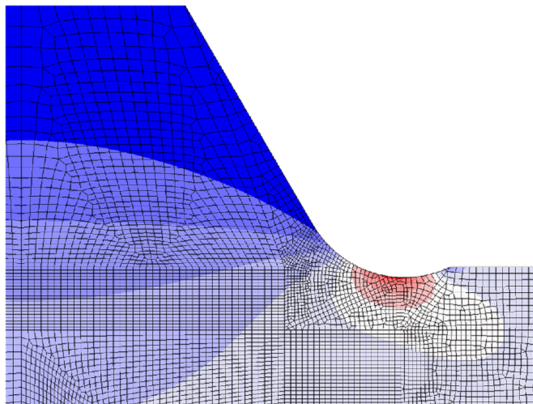


Fig. 7. Example of the 2D plane strain FE model used in effective notch stress analysis.

3. Numerical simulations for fatigue life comparisons

3.1. Case study for normal and high-performing welds

The numerical investigation is carried out on butt-welded joints with varied weld geometry. The plate thicknesses investigated are $t = 3$ mm and $t = 12$ mm in order to cover the typical plate thickness range of large welded structures. The study is focused on the effect of the weld shape, and thus axial and angular misalignments are not included. The same weld shape is used both for the weld toe and root side in order to avoid secondary bending stress for the original joint geometry. The effect of the weld shape is defined by the weld height h , width w , flank angle θ , undercut depth D , notch tip radius ρ , and opening angle β ; see Fig. 8. The butt joint is subjected to an axial load with a nominal stress $\sigma_{nom} = F/A$, where A is the cross-section area and F the applied force. In this study, the nominal stress σ_{nom} equals the structural stress σ_{hs} since the stress magnification factor is $k_m = 1$ as a result of non-existent misalignments and secondary bending stress. The nominal stress σ_{nom} also equals the nominal stress range $\Delta\sigma_{nom}$ since the load ratio of $R = 0$ is used in the analysis.

Three different weld geometries are considered to study the effect of the weld shape. The geometries that are studied are based on the statistical analysis of the systematic geometry measurements for laser and laser-hybrid welds; see [12,18], and [27]. On the basis of the analysis of the relationship between the geometrical dimensions of the weld and its fatigue strength – see e.g. [18,24] – the variation of the weld geometry is defined with the weld flank angle, weld height, and undercut depth. Other weld dimensions are kept constant and scaled according to the thickness of the plate in order to achieve a consistent thickness effect analysis. The three different cases are defined on the basis of the analysis of the weld geometry statistics: Case 1) a high-performing weld (upper bound geometry), Case 2) a high-performing weld (lower bound

geometry), and Case 3) a normal weld with a 0.1-mm undercut. As shown in Table 1, Case 1 is the smooth weld geometry with a flank angle of 5°. Case 2 represents a high-performing weld geometry with a flank angle of 20°. Case 3, i.e. the normal weld, has a flank angle of 60° and a 0.1-mm-deep undercut, representing the laser or laser-hybrid welds which has significant imperfections, but still fulfilling the fatigue strength requirements given in fatigue design recommendations; see [24]. The material properties of the joints under study are given in Table 2. The young modulus of 210 GPa and Poisson's ratio of 0.3 were assumed, while the material plastic behaviour was defined based on monotonic and cyclic loading tests of laser-hybrid welded normal-strength steels, see [51]. For the narrow heat-affected-zone (HAZ), the value of mechanical properties are interpolated using the measured hardness distribution as abscissa; see [35]. The microstructure characteristics were determined based on statistical analysis of Vicker's hardness test and grain size measurements using intercept length method. It is worth to notice that the plastic properties and microstructure characteristics are used only for SCG analysis, since other local approaches (LEFM, SED, ENS) use linear elastic material model. In SCG analysis, the fatigue crack can initiate and grow into HAZ or PM material, depending which one is more critical and gives shorter fatigue life.

3.2. Details regarding the modelling approaches

Depending on the method, the analysis details varied because of differences in the modelling assumptions. The guidelines for FEA were used, if available. The strain-based crack growth (SCG) analysis used a very fine mesh at the weld notch and crack tip; the minimum mesh size was in the order of 1 μm. The analyses were carried out using 2D Finite Element analysis and Abaqus Version 6.8-1. The use of 2D assumption is motivated by the experimental observations and numerical 3D simulation. For modern welding, the defect depth/length ratio is observed varied from 1:20 to 1:10. In such cases, the 3D effect is not significant; see [54]. Furthermore, the edge crack behaviour is observed for the fracture surfaces of the high-performing full-scale structures shown in Fig. 1; see [11]. The fatigue life prediction in SCG uses the average material coefficients, and thus it corresponds to the 50% survival probability level. To make predictions on the survival probability level of 97.7%, the fatigue life was divided by the safety factor F . The value F was defined on the basis of the statistical variation observed for crack initiation and propagation in the literature. In the case of crack initiation life, a statistical study for hardness-based prediction in [55] shows that an F -factor of 3 is a good assumption, corresponding to a survival probability level between 95.9% and 98.6%. On the basis of the BS7910 standard [56], the growth rate of long crack propagation is $C = 1.26^{-11}$ and $C = 2.14^{-11}$ [$1/(MPa^{2.88}\sqrt{m} \cdot cycle)$] for survival probability levels of 50% and 97.7%, respectively. Then the ratio of these values i.e. F -factor for propagation gets $F = 1.7$. Assuming that the crack propagation time is 60% of the total fatigue life according to [57], the F value for the current analysis becomes 2.22 ($0.4 * 3 + 0.6 * 1.7$). This value is in agreement with the IIW fatigue recommendation, which gives an F value within the range of 2–3. Thus, the F -value of 2.2 was used in the current study to correct the SCG mean fatigue life prediction to survival probability level of 97.7%. It is worth to notice that in SCG analysis the C values from BS7910 are only used here for the definition of F -factor, not for fatigue life calculations.

In LEFM the stress intensity factor K_I was calculated using the FRANC 2D software. The original weld geometry of the FE models was modified in such a way that an initial crack was added to the weld notch or undercut tip. The FE model consisted of parabolic plane-strain elements and the mesh at the crack tip was very fine. The minimum element size was 0.005 mm near the crack tip. For the thick plate, the crack propagation increment was 0.01 mm up to a crack length of 2 mm and afterwards 0.1 mm until the critical crack length was reached. These crack propagation increments were four times smaller for the

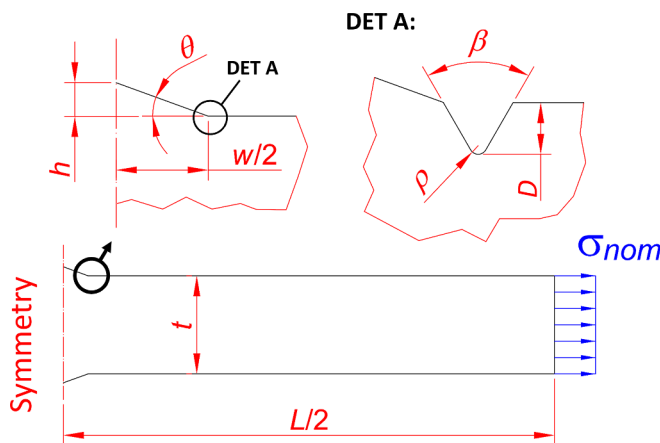


Fig. 8. The geometrical dimensions of a butt-welded joint.

thin plate. Fig. 9 presents the calculated stress intensity factors K_I as a function of crack length for the nominal stress of 100 MPa. The results are presented for actual crack length a , starting from crack length of 0.01 mm in order to illustrate better the influence of weld geometry and plate thickness on K_I values. For both thick and thin plates, the weld geometry has a significant influence on the K_I values when the crack length is smaller than 0.5 mm. Furthermore, the K_I values are different for thick and thin plates as a result of scale effects. For short cracks ($a < 0.2$ mm), the K_I values are higher for thick plates because of the larger weld size. For the upper-bound geometry of a high-performing weld (Case 3), the K_I values are almost equal for thin and thick plates since the weld is very smooth and the weld effect is negligible. These differences in the K_I values, as a function of crack length, resulted in differences in fatigue life calculated according to Eq. (4). In the fatigue life calculations, the material coefficient $C = 1.65^{-11}$ [1/(MPa $^3\sqrt{m} \cdot$ cycle)] and $n = 3$ were used according to the IIW recommendations [32]. It was also considered that if the range of stress intensity ΔK_I is less than the threshold value $\Delta K_{th} = 5.4$ MPa \sqrt{m} , the crack growth rate is zero and the fatigue life is infinite, defining the fatigue strength for two million load cycles. An initial crack size of $a_i = 0.1$ mm was assumed, and the critical crack length a_{cri} was defined by the limit load theory. According to this theory for tensile loading, the final failure occurs when the nominal stress of the cracked cross-section equals the ultimate strength of the material.

In order to evaluate the averaged SED for the applied load level and structural stress range, the numerical FE simulations under linear elastic conditions were carried out using the ANSYS® APDL15.0 finite element software package. The 2D plane strain element (PLANE183) and a coarse mesh [58] were employed. Indeed, in contrast to other methods, the SED approach did not require a fine mesh, since the strain energy density values were numerically evaluated solely from nodal displacements. As shown by Eq. (5), the fatigue assessment was carried out only in terms of energy. However, to facilitate a comparison with the other methods presented here, an S-N curve was derived. For the

Table 2
Mechanical properties applied in the numerical simulations.

Mechanical property	Parent material (PM)	Heat-affected zone (HAZ)
Young's modulus E [GPa]	210	
Poisson's ratio ν	0.3	
<i>Monotonic loading</i>		
Yield strength σ_y [MPa]	287	346
Tangent modulus E_T [MPa]	1650	1631
<i>Cyclic loading</i>		
Strain-hardening coefficient K [MPa]	794	906
Strain-hardening exponent n	0.143	0.144
<i>Microstructure characters</i>		
Hardness (HV5)	131	207
Average grain size d (μm)	9	2
Grain size at $P = 99\%$ $d_{99\%}$ (μm)	31	10

SED approach the averaged strain energy density range ΔW , corresponding to a survival probability of 97.7% and two million load cycles, is $\Delta W_a = 0.058$ MJ/m³ for the loading ratio $R = 0$ [45]. The inverse slope for the ΔW -life curve is $k = 1.5$ in terms of energy, and corresponds to a slope value $m = 3$ for the S-N curve. The ΔW -life curve of the SED analysis does not consider misalignments, as stated by Fischer *et al.* [59]. Thus, the stress of the S-N curve obtained by SED was multiplied by the stress magnification factor $k_m = 1.25$ according to [32] in order to make it comparable to the results of other methods. It is also worth mentioning that the averaged SED was originally developed for plate thicknesses above 5 mm. However, in this work, the SED approach is also applied to 3-mm-thick plates in order to study its applicability to thin plates.

The effective notch stress (ENS) approach, similarly to other methods, used the finite element method and 2D plane strain elements. The notch stress analysis and the definition of element mesh size that was used follow the IIW guidelines, [32,50]. Fig. 10 shows the fatigue notch factor K_f , i.e. the ratio between the maximum principal stress and the nominal stress σ_{nom} for the 1-mm rounding radius. It is clearly visible that the fatigue notch factor increases as a function of notch severity, having the highest value for the normal weld (Case 3). The notch factor is also higher for the thick plate as a result of the larger weld size and constrain effect. In the case of the thin plate, all values are lower than the minimum value $K_f = 1.6$ recommended by the IIW [50]. On the basis of the maximum principal stress at the notch tip, the fatigue life was calculated using the S-N curve with the slope value $m = 3$ and fatigue strength FAT225, corresponding to a survival probability of 97.7% [50]. Since this original FAT value is for the load ratio $R = 0.5$, it was multiplied by a mean stress correction factor of 1.1 according to [53] in order to consider the load ratio $R = 0$. Since the use of a 1-mm fictitious radius is not recommended for plate thicknesses < 5 mm [32], a radius of 0.05 mm was additionally used for comparison. In this case, the fatigue life was calculated using an S-N curve with FAT630 and the slope value $m = 3$, according to [50].

Table 1
Weld geometry cases considered in the analysis.

Weld	Plate thickness t of 3 mm			Plate thickness t of 12 mm		
	Dimensions	Case 1	Case 2	Case 3	Case 1	Case 2
Plate thickness t [mm]	3	3	3	12	12	12
Height h [mm]	0.07	0.27	1.3	0.26	1.09	5.2
Width w [mm]	1.5	1.5	1.5	6	6	6
Flank angle θ [degree]	5	20	60	5	20	60
Undercut depth D [mm]	0	0	0.1	0	0	0.1
Notch angle β [degree]	–	–	60	–	–	60
Notch tip radius ρ [mm]	–	–	0.02	–	–	0.02

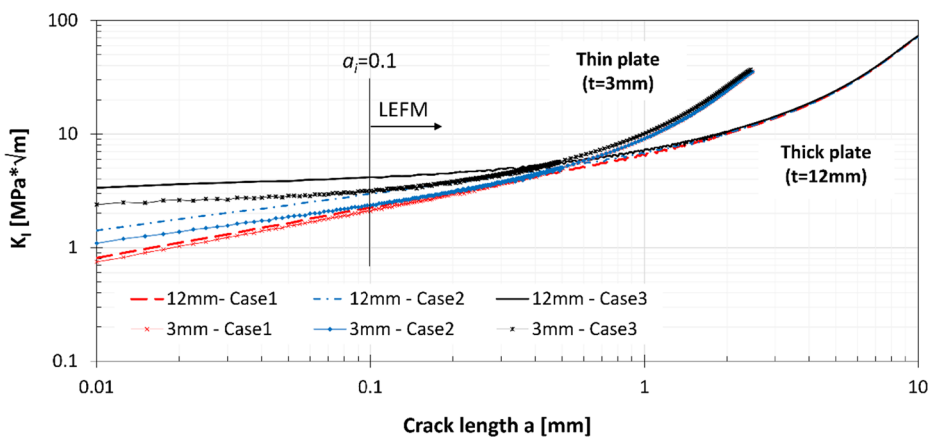


Fig. 9. Stress intensity factors K_I as a function of crack length for an external load of 100 MPa.

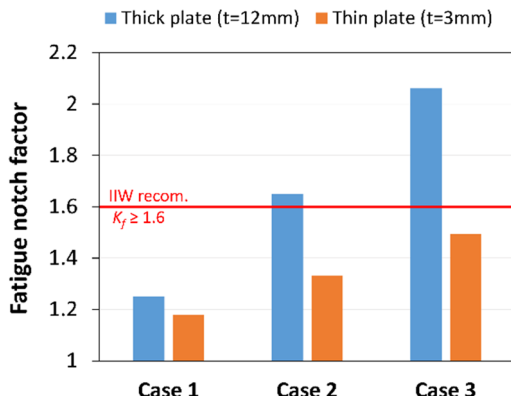


Fig. 10. The calculated fatigue notch factors for the weld geometries studied using the ENS approach.

3.3. Experimental data for results comparison

The fatigue life predictions from different local approaches are compared to each other, but also with the experimental data taken from literature; see refs [25,27], and [32] at the survival probability level of 97.7%. The calculated fatigue life is plotted as a function of structural stress to consider possible influence of the misalignment on the results comparison. In the case of the local approaches the structural stress equals to nominal stress since the case study models are symmetric without misalignments. Thus, the results of local approaches and experimental reference data is presented in term of structural stress. For the normal weld, i.e. Case 3, the fatigue class FAT100 with a slope of $m = 3$ was used [32]. Since the FAT100 class is based on the statistical analysis of an extensive experimental database, the individual data points are, for simplicity, not presented here. Similarly to the S-N curve for the notch stress approach, this FAT value is for the load ratio of $R = 0.5$, and it was corrected for the load ratio $R = 0$ with a stress correction factor of 1.1 according to [53]. For high-performing welds common FAT class does not exist and thus, the fatigue test data for

laser-hybrid welded thick and thin plates is taken from the previous studies, [25,27]. The fatigue test data was obtained for plate thicknesses of 12 mm and 4 mm, assuming that the fatigue strength of 4-mm and 3-mm welded plates is similar when the comparison of the results is performed in the structural stress system, i.e. the secondary bending stress resulting from misalignment is considered independently; see [60]. Fig. 11 shows the macro-sections of these welds. The weld bead height is small or moderate. In all welds, the weld notch shape is smooth and an undercut is not observed. Thus, the geometry of these experimental results corresponds to the high-performing welds (Case 1 and 2). Using the fixed slope $m = 5$, the characteristic fatigue strength of these reference welds is 202 MPa and 219 MPa for thick and thin plate, respectively. The slope $m = 5$ shows good fit to the experimental data of thin plate while for thick plate with smaller weld size higher slope value can be also fitted to the fatigue test data. Then, the characteristic fatigue strength of thick plate is 253 MPa.

4. Results

4.1. Comparison of predicted S-N curves

Fatigue life predictions for the total fatigue life are presented in Figs. 12 and 13 as S-N curves for the stress-based local approaches (ENS, SED, $R_{ref} = 0.05$ mm) and the crack growth approaches (LEFM, SCG). Furthermore, the characteristic fatigue strength value at 2 million load cycles are given. The predicted curves are compared to fatigue test data for the high-performing welded joints from [25,27], as well as to the S-N curve of the structural stress approach (FAT100, $m = 3$) according to [32] as described in Section 3.3. A general observation is that all the approaches that are considered predict an increased fatigue strength for the high-performing welds (Case 1 and 2 i.e. the lower and upper bound geometry) in comparison to the normal weld (Case 3). However, significant variation is observed between the methods and plate thicknesses.

Fig. 12a-b shows the S-N curves for the ENS approach applied to thick and thin plates. For the normal weld in a thick plate (Case 3,

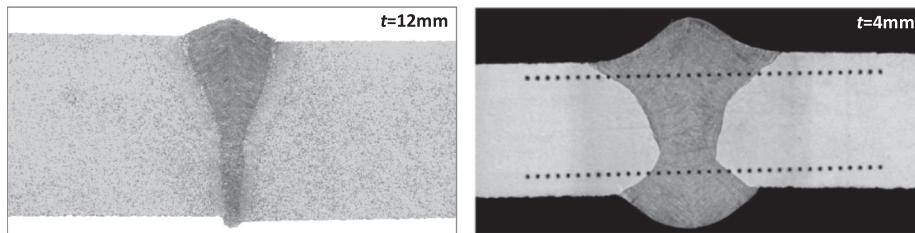


Fig. 11. A macro section of high-performing welds in thick and thin plates.

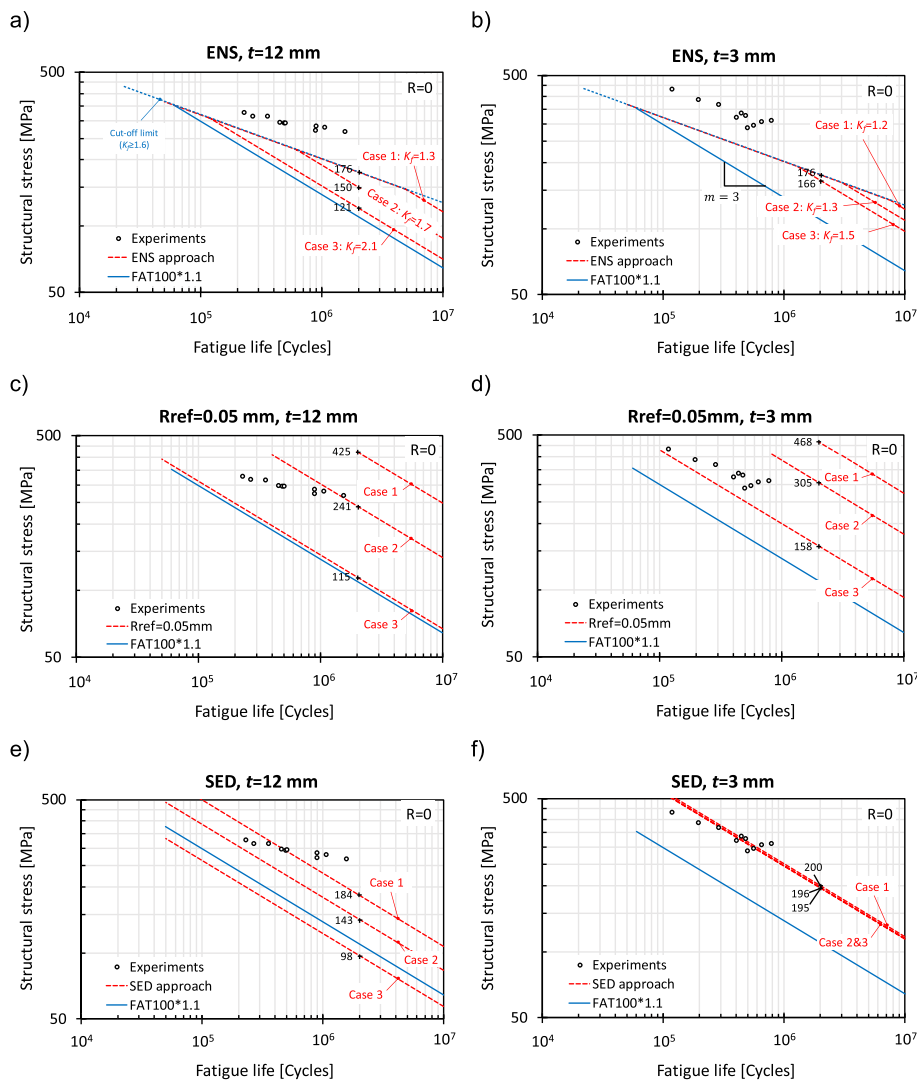
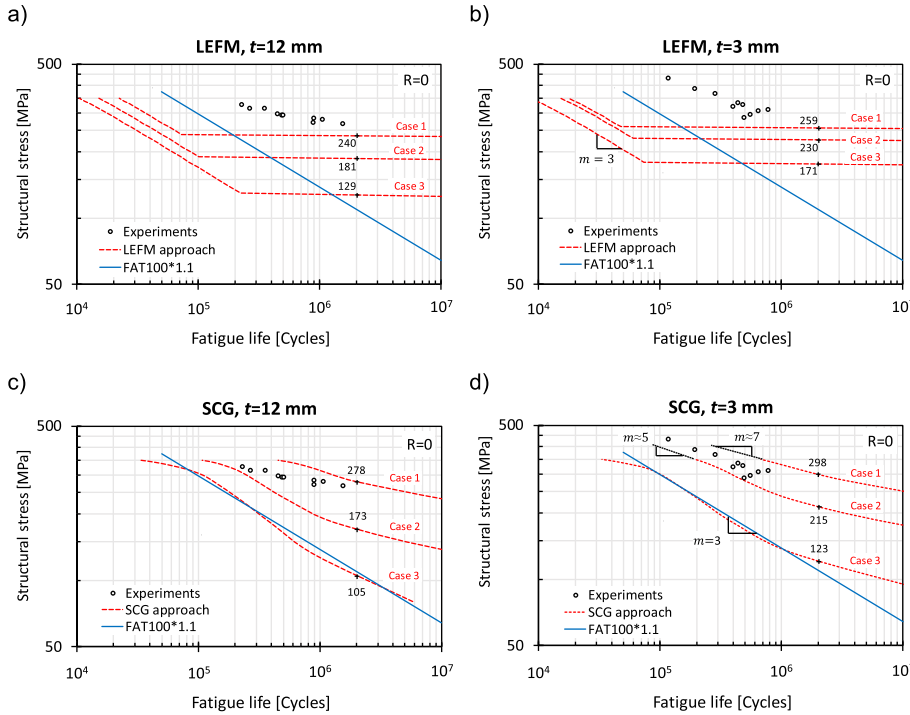


Fig. 12. Predicted S-N curves and characteristic fatigue strength values using stress-based local approaches (a-b) ENS, (c-d) $R_{\text{ref}} = 0.05 \text{ mm}$, (e-f) SED for high-performing (Case 1 and 2) and normal (Case 3) welds. The FAT100 design curve for the normal weld and the fatigue test data for the high-performing weld (circle symbol) are given for comparison.

$t = 12 \text{ mm}$), the predicted S-N curve is close to the structural stress S-N curve (FAT100*1.1). The S-N curves are also higher for the high-performing welds (Cases 1 and 2) than expected, although on the conservative side. For the thin plate, the S-N curve for the normal weld is significantly higher than the structural stress S-N curve, having the characteristic fatigue strength of 166 MPa. The S-N curves for the high-performing welds (Cases 1 and 2) are slightly higher in comparison to the S-N curves for a thick plate. For both thick and thin plates, the cut-off limit (blue dashed line shown in Fig. 12a-b) defines the fatigue strength in the medium-cycle fatigue range ($N < 10^6$). This cut-off limit is introduced in the IIW notch stress guidelines [50] to represent the maximum allowed fatigue strength for low K_f values, assuming that the defects in the parent material define the fatigue strength of the welded joint. On the basis of the comparison of the S-N curves and test data, the ENS approach seems to give a conservative prediction for the high-performing welds, and a non-conservative prediction for the normal weld in a thin plate. If the fictitious rounding radius of 0.05 mm ($R_{\text{ref}} = 0.05 \text{ mm}$) is applied instead, the fatigue strength predictions at two million load cycles are reasonable for the thick plate (Fig. 12c) and non-conservative for thin plates (Fig. 12d). Furthermore, the fixed slope of $m = 3$ makes the estimation non-conservative when $N < 10^6$ cycles in the case of high-performing welds. The SED gives similar or slightly

lower fatigue strength predictions at two million load cycles for the thick plate in comparison to ENS and $R_{\text{ref}} = 0.05 \text{ mm}$. Similarly to $R_{\text{ref}} = 0.05 \text{ mm}$, the fixed slope of $m = 3$ makes the prediction non-conservative when $N < 10^6$ cycles in the case of high-performing welds (Case 1 and 2). For the thin plate (Fig. 12f), the averaged SED is not able to make a distinction between the different weld cases, but the prediction for high-performing welds seems to agree with the average of the experimental data.

Fig. 13 shows the S-N curve predictions to crack growth approaches. The S-N curves predicted by LEFM are presented in Fig. 13a-b. The fatigue strength at two million load cycles (i.e. at the endurance limit) is slightly conservative for high-performing welds (Case 1 and 2) as the predicted S-N curves are well below of the experimental data. For normal weld (Case 3), the predicted fatigue strength at two million load cycles is too high especially in the case of thin plate, being well above of the FAT100 reference curve. In the zone of the medium-cycle fatigue ($10^4 < N_f < 10^6$), the predicted fatigue life is distinctly conservative for all cases and both plate thicknesses. It is worth noticing that the fatigue life predictions of LEFM do not include the crack initiation period since an initial crack size is used as a starting point. In contrast to LEFM, the strain-based crack growth (SCG) includes crack initiation and the short crack growth. Then, as shown in Fig. 13c-d, the predicted



S-N curve for the normal weld (Case 3) is well in line with the structural stress S-N curve (FAT100), being similar to ENS and SED for a thick plate with a fixed slope value $m = 3$. For the high-performing welds (Case 1 and 2), the predicted S-N curves are significantly higher in comparison to the normal weld (Case 3), being more similar to the experiments with higher S-N curve slope values. The slope of the S-N curves varies according to the weld shape from 3 (Case 3) up to 7 (Case 1), indicating the increasing importance of the crack initiation time for high-performing welds. These results indicate that the macro-crack initiation time, up to 0.1 or 0.2 mm in crack length, is significant for a weld with a smooth geometry.

4.2. The influence of weld shape on crack initiation behaviour

In order to understand the influence of weld shapes on macro crack initiation, the fatigue life accumulation as a function of crack length is studied using the strain-based SCG approach. Fig. 14 shows the portion of fatigue cycles accumulated in different crack length ranges ($0\text{--}0.1\text{ mm}$, $0.1\text{--}0.2\text{ mm}$, ..., $1\text{--}a_{\text{cri}}$). Fig. 14 shows the proportions for the selected stress ranges $\Delta\sigma$ of 130 MPa and 280 MPa, corresponding to low-cycle and high-cycle fatigue behaviour. The results for $\Delta\sigma = 130\text{ MPa}$ show that for the high-performing welds (Case 1 and 2) most of the fatigue life is spent on crack growth up to a crack size of 0.1 mm. In the normal weld with a 0.1-mm undercut (Case 3), the

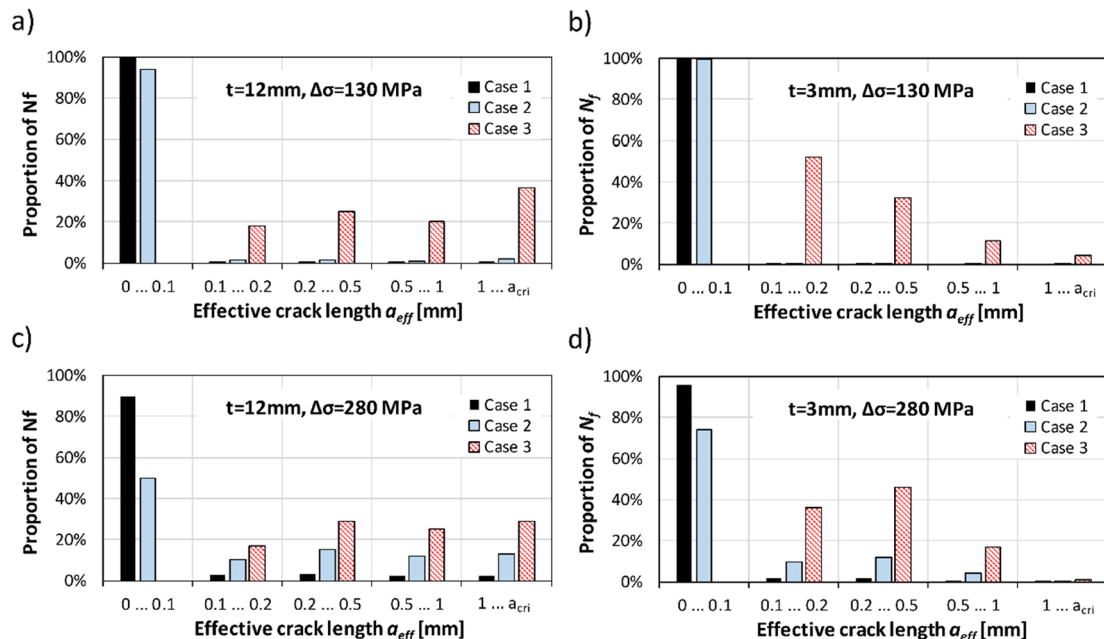


Fig. 14. Crack growth time between different crack lengths in comparison to the total fatigue life N_f for the stress range of $\Delta\sigma = 130\text{ MPa}$ (a-b) and $\Delta\sigma = 280\text{ MPa}$ (c-d).

proportion of the total fatigue life N_f is somewhat similar for different crack length ranges, illustrating the greater importance of macro crack propagation, as expected. The results for the higher-stress range $\Delta\sigma$ of 280 MPa show a similar trend, but the importance of crack propagation is increased in all cases. This is clearly visible for the thick plate and high-performing weld (Case 2), where the proportion of the total fatigue life N_f for a crack length 0–0.1 mm is reduced from 94% to 50%.

4.3. The influence of weld shape on crack growth behaviour

The differences in short crack growth are studied by plotting the fatigue crack growth rate, computed from SCG analysis using Eq. (3), as a function of the stress intensity factor range ΔK_I . In the calculation of ΔK_I , the effective crack length ($a_{eff} = D + a + d_{99\%}$) is used, i.e. the initial crack size is equal to the undercut depth D and the size of RVE i.e. $d_{99\%}$. As shown in Fig. 15, the estimated crack growth rate (CGR) is similar for all cases and load levels. However, the starting point of the CGR curve is different for high-performing and normal welds, since the initial stress intensity factor ΔK_I depends on the weld notch shape effect. For the high-stress range ($\Delta\sigma = 280$ MPa) and the normal weld (Case 3), the crack growth started directly from the Paris' law regime (marked A-B) and continues as a tearing-dominated crack growth; see Fig. 15. In the case of the high-performing welds (Case 1 and 2) and low nominal stress range ($\Delta\sigma = 130$ MPa), the short crack growth period before the Paris' law regime (left of A) is more important. In this case, the LEFM with a selected threshold value $\Delta K_{th} = 5.4 \text{ MPa}\sqrt{m}$ (IIW) is highly conservative since it does not include the CGR curve in the short crack growth domain. In the case of high-performing welds (Cases 1 and 2), the thickness effect is clearly visible only in the early stages of crack growth. The CGR of a short crack in the thin plate is lower in comparison to the thick plate with a larger weld size.

5. Discussion

It is well known that crack nucleation constitutes a significant portion of the total fatigue life for polished bulk material. The crack nucleation time is taken as the time for micro cracks to coalesce into a short crack. Then the fatigue damage process is followed by short crack growth and, subsequently, long crack propagation until final fracture; see e.g. [61]. Therefore, for polished material, the modelling of fatigue damage needs to focus on the mechanics on the microstructural scale, applying the similitude concept for dislocation movements and their accumulation during cyclic loading [8]. However, depending on the engineering application, the assumptions for the similitude concept can vary. For welded joints, these assumptions are mainly dependent on the

size of the notch and undercut, and their influence on the plastic deformation behaviour. For instance, crack-like defects, i.e. undercuts in normal welds, lead to short crack initiation times, with crack propagation dominating the fatigue life. For high-performing welds, the crack initiation time can form a major part of the total life. Although the experimental observation of short crack growth is very challenging, the literature indicates that as much as 80% of the fatigue life can be spent on initiating a macro crack in welded components; see e.g. [41]. Consequently, there is a fundamental difference in the mechanics, growth rate, and fatigue damage accumulated between low- and high-performing welds, as shown in Figs. 14 and 15. The former is dominated by long crack propagation, while the latter is dominated by short crack initiation and growth. This fact challenges the fundamental assumptions used in different existing local approaches based on the concept of similitude.

For short crack growth, the crack tip plasticity is limited to a region in the order of the average grain size as shown in meso-scale modelling [9] and recent in situ grain-level DIC measurements for a high-cycle fatigue regime [62]. Since the SCG model uses a microstructure-dependent RVE based on the grain size statistics, it models this fatigue behaviour implicitly using continuum theory and the averaged RVE value for plastic deformation and damage growth rate. For short cracks, the size of the plastic zone is smaller than that of the RVE, while for long cracks the size of the plastic zone is larger than that of the RVE, resulting in differences in the rate of fatigue damage and crack growth rate; see e.g. [34]. Since the actual stress state and plasticity outside the RVE during crack growth are explicitly considered in the FE analysis, SCG is able to predict the changes in the crack growth rate and the S-N curve slope as a function of weld geometry and load levels (Fig. 13). Out of all the approaches that were investigated, SCG is the only one that predicts a bilinear crack growth curve (Fig. 15) with a flatter S-N curve slope in the high-cycle regime. This prediction is in good agreement with crack growth experiments and the BS 7910 standard [56], which recommends two-stage crack growth relationships for accurate crack growth analysis. Thus, the current results indicate that the similitude concept based on a microstructure-dependent RVE is suitable for the fatigue modelling of high-performing welded joints. The complementary evidence for this finding might be obtained from numerical meso-scale analysis and Monte-Carlo simulations that cover different grain sizes as well as grain interactions.

For linear elastic fracture mechanics (LEFM), the similitude concept is based on the material constraint effect, assuming that the crack always has the same shape of stress gradient and stress/strain state, resulting in similarity in its plasticity behaviour. Thus, these effects can be considered generic between different crack cases and they can be

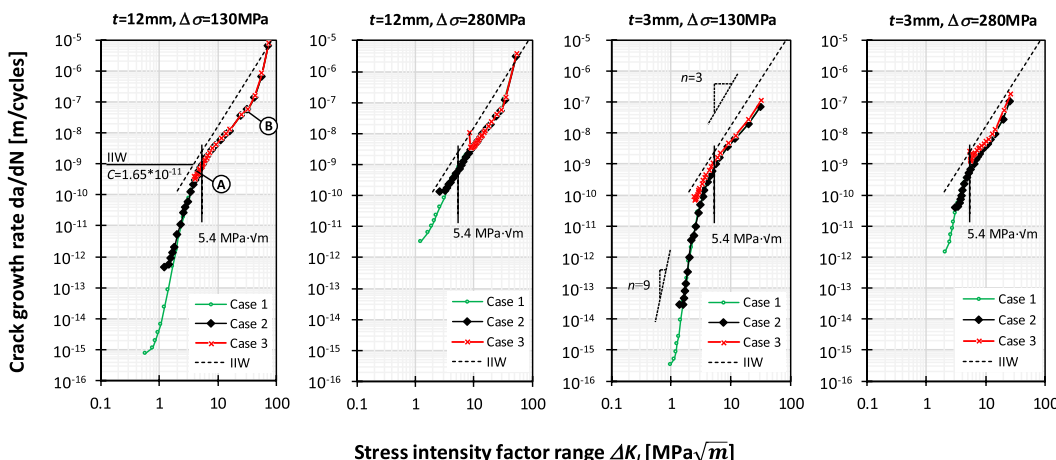


Fig. 15. Simulated fatigue crack growth rate CGR as a function of the stress intensity factor for different weld shapes (Case 1–3), stress ranges ($\Delta\sigma = 130$ MPa, 280 MPa), and plate thicknesses ($t = 3$ –12 mm). IIW design values for crack propagation analysis using LEFM are given for comparison. The markers A and B denote

modelled with experimentally defined material constants. As shown in Fig. 13, LEFM gives a somewhat good prediction for the endurance limit of high-performing welds (Cases 1 and 2). This might be a consequence of the endurance limit prediction being related to the threshold of crack propagation as shown e.g. in [64] and the initial crack size used. However, fatigue life prediction in the finite life regime is a challenge since the macro-crack initiation period is neglected in LEFM. The predictive capabilities of LEFM can be improved by using a bi-linear crack growth model, as recommended in the BS 7910 standard [56]. In this approach the threshold stress intensity factor is not used, while different crack growth coefficients and exponents are used above and below a stress-intensity factor of $\Delta K = 5.4 \text{ MPa}\sqrt{m}$. Another alternative is to use so-called fatigue crack initiation and propagation approach, where LEFM is used for crack propagation; see e.g. [63]. However, the definition of the initial crack size for LEFM is challenging for a high-performing weld. It should also be noted that the use of a fictitious crack size violates the basic assumptions and similitude concept used in LEFM.

The similitude concept of LEFM is developed further for the averaged strain energy density approach. The shape of the weld notch is modelled as a sharp V-shaped notch and it is assumed that the crack initiation life associated with the initial geometry dominates the fatigue strength prediction at the endurance limit. With these assumptions, the fatigue strength can be predicted for the infinite fatigue life regime using an experimentally defined, unified W-N curve similar to the original Wöhler curve concept. The control volume required for the prediction is defined on the basis of the mechanical properties of welded joints. For the arc-welded joints in the plate with a thickness of more than 5 mm, a fixed average volume of $R_o = 0.28 \text{ mm}$ is recommended for engineering use. On the basis of the current results, it seems that this value is not optimal for thin plates and additional precautions should be taken to consider the slope changes. It should be noted that the averaged SED approach fully includes the scale effect. However, this effect is dependent on the plate thickness and the opening angle (i.e. William's eigenvalue), as shown in [45]: the smaller the flank angle, the smaller the scale effect. This might explain why the thick and thin plates of Case 1 have similar fatigue strength predictions, while the variation increases for Case 2 and Case 3. Similarly, the ENS depends on the plate thickness, since the similitude concept that is applied is based on the stress solution for an elliptical notch in a finite plate [52]. Because the stress-state is not fully developed for thin plates, there are differences in the stress distribution and plastic deformation behaviour at the weld notch tip, as shown e.g. in [29,66]. This effect of thickness on ENS predictions has been shown in previous studies and the use of a smaller radius of 0.05 mm is recommended. In this case, the stress gradient effects in the small control volume need to be considered carefully and, as a consequence, a different unified S-N curve has been proposed by Kranz and Sonsino for low-stress concentrations [53]. According to this proposal, if e.g. the FAT400 fatigue class is applied instead of FAT630, a 36% reduction is observed in the fatigue strength prediction. This correction is suitable for thin plates, but leads to non-conservative predictions for thick plates, especially for a normal weld with a sharp undercut (Case 3). Similar challenges for the notch stress approach with a fictitious rounding have been reported by Baumgartner [65], and he suggested the use of FAT160 with a slope value of $m = 5$. This conservative approach is rational for engineering purposes, but is of limited applicability to the fatigue strength modelling of high-performing welds. It is worth noting that the use of 5 mm limit value is artificial without scientific basis and thus, it can lead to unexpected inconsistencies particularly near the limit value.

In spite of certain limitations of the conventional linear elastic local approaches such as SED and ENS, they are efficient methods for fatigue design of welded structures where normal weld quality can be guaranteed. Their master S-N curve, defined based on the large statistical database of different quality welds, includes implicitly the statistical uncertainties between different welds that are made using different

parent materials and welding technologies. The use of the elastic-plastic local approach, which is sensitive to microstructure such as SCG method, enables the explicit modelling of the weld quality, i.e. the geometry, material, and microstructure effects. Thus, the statistical variation can be considered explicitly as a model input data, enabling new possibilities for fatigue design. Consequently, SCG can predict better structural hot-spot stress S-N curves for different production precision and quality. Vice versa, SCG can be utilized to define requirements for superior production quality and NDT control methods for a new industrial project and application. Although, the SCG is more time-consuming than conventional local approaches, it can be used also in direct fatigue life assessment of industrial applications, by using sub-modelling technique; see [41].

6. Conclusions

In this paper, the effect of plate thickness and weld notch geometry on fatigue strength modelling was studied using the strain-based crack growth approach (SCG), linear elastic-fracture mechanics (LEFM), averaged strain energy density (SED), and the notch stress approach (ENS, $R_{ref} = 0.05 \text{ mm}$). In the strain-based crack growth approach, the fatigue damage process is modelled as a repeated crack initiation process using the microstructure-dependent representative volume element (RVE). This enables the changes in the crack tip plasticity to be considered and thus also the crack initiation and growth of a short crack until final failure. The results of the numerical simulations are compared to the fatigue test results of high-performing welds.

The study reveals that the macro crack initiation period becomes significant for high-performing welds with smooth or favourable notch geometry, causing inaccuracies with the commonly applied LEFM, averaged SED, ENS, and $R_{ref} = 0.05 \text{ mm}$ approaches as a result of the absence of the explicit modelling of the crack initiation and propagation periods. The fixed S-N curve slope value $m = 3$ or crack growth rate $n = 3$ are not a suitable assumption for a high-performing weld. With the strain-based SCG simulation, the crack initiation and short crack growth are modelled, resulting in a significant increase in the S-N curve slope value. Of the approaches that are considered, SCG is the only method that properly predicts a variation in the slope for different weld geometries. SED, ENS, and $R_{ref} = 0.05 \text{ mm}$ had challenges in capturing the stress gradient effect for thin plates and, thus, difficulty in applying the unified master-curve concept. These results indicate that their fictitious rounding radius or average volume does not represent the optimum values for thin plates.

The macro crack propagation becomes more significant for normal welds in thick plates, and thus, all the methods that were considered give a somewhat similar fatigue strength prediction at two million load cycles. The commonly used slope value of the S-N curve, $m = 3$, shows good agreement with the simulations. The results also reveal that LEFM and SCG give somewhat similar results for the fatigue strength at the endurance limit i.e. at 2 million load cycles in the case of high-performing welds. However, the fatigue life prediction in the medium-cycle range is over-conservative for LEFM. This is because LEFM predicts the fatigue strength at the endurance limit on the basis of the crack growth threshold, while the crack growth model without crack initiation time is used to predict fatigue life in the medium-cycle range. The ENS and SED approaches had difficulties in reliably predicting the fatigue life of normal welds in thin plates, resulting in predictions that were significantly higher than the FAT100 fatigue class. The results indicate that their fictitious rounding radius or average volume is not optimal either for normal welds in thin plates, i.e. when undercuts are present in the weld geometry.

An overall comparison of the different modelling approaches shows that a simplified modelling of the weld notch effect can cause significant uncertainties in the fatigue strength assessment of high-performing welds, even when secondary bending effects are not present. This is because the commonly used local approaches, such as ENS and

SED, assume a priori that the welded joints under consideration belong to the unified S-N or ΔW -life master curve population. This assumption implicitly means that the slope of the fatigue curves is fixed at a value of 3 in terms of stresses (or 1.5 in SED). Despite the fact that this holds true for a wide range of common welded joints, the fatigue data of high-performing welds clearly shows a different slope. Thus, the use of the more sophisticated strain-based SCG approach is required to develop a solid basis for the fatigue strength assessment of high-performing welds. Future work is required to cover different joint types and steel materials in order to obtain a more comprehensive understanding of the fatigue behaviour of high-performing welds. At present, the experimental data of high-performing welds, including their geometry and materials characterisation, is very limited and future research is needed in these areas. Future research is also needed for the modelling of very high cycle fatigue range.

Declaration of Competing Interest

The authors declare that they have no known competing financial interests or personal relationships that could have appeared to influence the work reported in this paper.

Acknowledgement

The present research was financially supported by the Academy of Finland (decisions nos. 298762 and 321244), the Finnish Funding Agency for Innovation, TEKES, and the Finnish metal industry. All the financial support is gratefully appreciated. Appreciation is also due to CSC – IT Centre for Science Ltd. for the allocation of computational resources.

References

- [1] Wöhler A. Über die Festigkeitsversuche mit Eisen und Stahl. *Zeitschrift Für Bauwes* 1870;20:73–106.
- [2] Basquin OH. The exponential law of endurance tests. In: Proc. ASTM; 1910, p. 625.
- [3] Schütz W. History of Fatigue. A history of fatigue. *Eng Frac Mech* 1996;54:263–300.
- [4] Coffin LF. A study of the effect of cyclic thermal stresses on ductile metal. *Trans ASME* 1954;76:931–50.
- [5] Manson SS. Behaviour of materials under conditions of thermal stress. Heat transfer symposium. University of Michigan, Engineering Research Institute and NACA TN2933; 1954: p. 9–74.
- [6] Paris PC, Gomez MP, Anderson WE. A rational analytic theory of fatigue. *Trend Eng* 1961;13:9–14.
- [7] Paris P, Erdogan F. A critical analysis of crack propagation laws. *J Basic Eng* 1963;85:528–33.
- [8] McDowell DL, Dunne FPE. Microstructure-sensitive computational modeling of fatigue crack formation. *Int J Fatigue* 2010;32:1521–42.
- [9] Li DF, Richard A, Barrett RA, O'Donoghue PE, O'Dowd NP, Leen SB. A multi-scale crystal plasticity model for cyclic plasticity and low-cycle fatigue in a precipitate-strengthened steel at elevated temperature. *J Mech Phys Solids* 2017;101:44–62.
- [10] Radaj D, Sonsino CM, Fricke W. Recent developments in local concepts of fatigue assessment of welded joints. *Int. J. Fatigue* 2009;31:2–11.
- [11] Remes H, Romanoff J, Lillemäe I, Frank D, Liinalampi S, Lehto P, et al. Factors affecting the fatigue strength of thin-plates in large structures. *Int J Fatigue* 2017;101:397–407.
- [12] Lillemäe I, Lammi H, Molter L, Remes H. Fatigue strength of welded butt joints in thin and slender specimens. *Int J Fatigue* 2012;44:98–106.
- [13] Eggert L, Fricke W, Paetzold H. Fatigue strength of thin-plated block joints with typical shipbuilding imperfections. *Weld World* 2012;56:119–28.
- [14] Fricke W, Remes H, Feltz O, Lillemäe I, Tchuindjang D, Reinert T, et al. Fatigue strength of laser-welded thin-plate ship structures based on nominal and structural hot-spot stress approach. *Ships Offshore Struct* 2015;10:39–44.
- [15] Frank D, Remes H, Romanoff J. Fatigue assessment of laser stake-welded T-joints. *Int J Fatigue* 2011;33:102–14.
- [16] Remes H, Fricke W. Influencing factors on fatigue strength of welded thin plates based on structural stress assessment. *Weld World* 2014;58:915–23.
- [17] Remes H, Peltonen M, Seppänen T, Kukkonen A, Liinalampi S, Lillemäe I, et al. Fatigue strength of welded extra high-strength and thin steel plates. In: Proceedings of MARSTRUCT 2015 – Analysis and design of marine structures, Southampton, UK; March 25th–27th 2015, London. pp. 301–308.
- [18] Lillemäe I, Remes H, Liinalampi S, Antti Itävuo A. Influence of weld quality on the fatigue strength of thin normal and high strength steel butt joints. *Weld World* 2016;60:731–40.
- [19] Caccese V, Blomquist PA, Berube KA, Webber SR, Orozco NJ. Effect of weld geometric profile on fatigue life of cruciform welds made by laser/GMAW processes. *Mar Struct* 2006;19:1–22.
- [20] Barsoum Z, Jonsson B. Influence of weld quality on the fatigue strength in seam welds. *Eng Fail Anal* 2011;18:971–9.
- [21] Radaj D, Sonsino CM, Fricke W. Fatigue assessment of welded joints by local approaches. Cambridge: Woodhead; 2006.
- [22] Remes H, Jelovica J, Romanoff J, Lehto P, Liinalampi S. Fatigue strength modelling of high-performance welds using local approaches. In: International Symposium on Practical Design of Ships and Other Floating Structures (PRADS), 2016, Copenhagen, Denmark.
- [23] DNV Classification Notes 30.7 (2014) Fatigue assessment of ship structures.
- [24] Remes H, Varsta P. Differences in fatigue strength between arc and laser hybrid welded joints. *J Ship Prod* 2008;24:139–45.
- [25] Lillemäe I, Liinalampi S, Remes H, Itävuo A, Niemelä A. Fatigue strength of thin laser-hybrid welded full-scale deck structure. *Int J Fatigue* 2017;95:282–92.
- [26] Jonsson B, Samuelsson J, Marquis G. Development of Weld Quality Criteria Based on Fatigue Performance. *Welding in the World* 2011;55:79–88.
- [27] Remes H, Varsta P. Statistics of Weld Geometry for Laser-Hybrid Welded Joints and its Application within Notch Stress Approach. *Weld World* 2010;54:R189–207.
- [28] Liinalampi S, Remes H, Lehto P, Lillemäe I, Romanoff J, Porter D. Fatigue strength analysis of laser-hybrid welds in thin plate considering weld geometry in micro-scale. *Int J Fatigue* 2016;87:143–52.
- [29] Gallo P, Guglielmo M, Romanoff J, Remes H. Influence of crack tip plasticity on fatigue behaviour of laser stake-welded T-joints made of thin plates. *Int J Mech Sci* 2018;136:112–23.
- [30] Gallo P, Remes H, Romanoff J. Influence of crack tip plasticity on the slope of fatigue curves for laser stake-welded T-joints loaded under tension and bending. *Int J Fatigue* 2017;99:125–36.
- [31] Barsoum Z. Fatigue Design of Welded Structures — Some Aspects of Weld Quality and Residual Stresses. *Welding World* 2011;55:2–11.
- [32] Hobbacher AF. Recommendations for fatigue design of welded joints and components. International Institute of Welding: Springer; 2016.
- [33] ISO 5817:2014 Welding – Fusion-welded joints in steel, nickel, titanium and their alloys (beam welding excluded) – Quality levels for imperfections; 2014.
- [34] Remes H, Varsta P, Romanoff J. Continuum approach to fatigue crack initiation and propagation in welded steel joints. *Int J Fatigue* 2012;40:16–26.
- [35] Remes H. Strain-based approach to fatigue crack initiation and propagation in welded steel joints with arbitrary notch shape. *Int J Fatigue* 2013;52:114–23.
- [36] Remes H, Lehto P, Romanoff J. Microstructure and Strain-Based Fatigue Life Approach for High-Performance Welds. *Adv Mater Res* 2014;891–892:1500–6.
- [37] Lehto P, Remes H, Saukkonen T, Hänninen H, Romanoff J. Influence of grain size distribution on the Hall-Petch relationship of welded structural steel. *Mater Sci Eng A* 2014;592:28–39.
- [38] Lehto P. Grain size measurement using Matlab. Aalto University wiki page. Available: <https://wiki.aalto.fi/display/GSMUM/>; 2016. Viewed 13.8.2019.
- [39] Hall EO. The Deformation and Ageing of Mild Steel: III Discussion of Results. *Proc Phys Soc, Section B* 1951; 64: 747–753.
- [40] Petch NJ. The cleavage strength of polycrystals. *J Iron Steel Inst* 1953;174:25–8.
- [41] Garcia M, Nussbaumer A, Remes H. Strain-based approach to fatigue crack initiation on high-strength-steel welded joints under multiaxial loading. The Seventh International Conference on Structural Engineering, Mechanics and Computation; 2019, Cape Town, South Africa.
- [42] Smith KN, Watson P, Topper TH. Stress-strain function for the fatigue of metals. *J Mater* 1970;5:767–78.
- [43] Roessle ML, Fatemi A. Strain-controlled fatigue properties of steels and some simple approximations. *Int J Fatigue* 2000;22:495–511.
- [44] Williams ML. On the Stress Distribution at the Base of a Stationary Crack. *J Appl Mech* 1956;24:109–14.
- [45] Lazzarin P, Zambardi R. A finite-volume-energy based approach to predict the static and fatigue behavior of components with sharp V-shaped notches. *Int J Fract* 2001;112:275–98.
- [46] Berto F, Lazzarin P. A review of the volume-based strain energy density approach applied to V-notches and welded structures. *Theor Appl Fract Mech* 2009;52:183–94.
- [47] Berto F, Lazzarin P. Recent developments in brittle and quasi-brittle failure assessment of engineering materials by means of local approaches. *Mater Sci Eng R Reports* 2014;7(5):1–48.
- [48] Lazzarin P, Lassen T, Livieri P. A notch stress intensity approach applied to fatigue life predictions of welded joints with different local toe geometry. *Fatigue Fract Eng Mater Struct* 2003;26:49–58.
- [49] Livieri P, Lazzarin P. Fatigue strength of steel and aluminium welded joints based on generalised stress intensity factors and local strain energy values. *Int J Fract* 2005;133:247–76.
- [50] Fricke W. IIW Recommendations for the Fatigue Assessment of Welded Structures by Notch Stress Analysis. International Institute of Welding, Woodhead Publishing; 2012.
- [51] Remes H. Strain-based approach to fatigue strength assessment of laser-welded joints. Doctoral dissertation, Helsinki University of Technology, Department of Mechanical Engineering, Espoo; 2008.
- [52] Neuber H. Über die Berücksichtigung der Spannungskonzentration bei Festigkeitsberechnungen (On the consideration of stress concentrations in strength analyses). *Konstruktion* 1968;20:245–51.
- [53] Sonsino CM. A consideration of allowable equivalent stresses for fatigue design of welded joints according to the notch stress concept with $r_{ref} = 1.00$ mm and 0.05 mm. *Weld World* 2009;53:R64–75.
- [54] Liinalampi S, Remes H, Romanoff J. Influence of three-dimensional weld undercut

- geometry on fatigue-effective stress. *Weld World* 2019;63:277–91.
- [55] Lee K-S, Song J-H. Estimation methods for strain-life fatigue properties from hardness. *Int J Fat* 2006;28:386–400.
- [56] BS 7910:2013. Guide to methods for assessing the acceptability of flaws in metallic structures. London: British Standards Institution; 2013.
- [57] Remes H. Fatigue tests of CO₂-laser, CO₂-laser hybrid and submerged arc welded butt joint of RAEX S275 LASER and NVA. Research Report M-278. Espoo, Finland: Helsinki University of Technology, Department of Mechanical Engineering; 2003.
- [58] Lazzarin P, Berto F, Zappalorto M. Rapid calculations of notch stress intensity factors based on averaged strain energy density from coarse meshes: Theoretical bases and applications. *Int J Fatigue* 2010;32:1559–67.
- [59] Fischer C, Fricke W, Rizzo CM. Review of the fatigue strength of welded joints based on the notch stress intensity factor and SED approaches. *Int J Fat* 2016;84:59–66.
- [60] Fricke W, Remes H, Feltz O, Lillemäe I, Tchuindjang D, Reinert T, et al. Fatigue strength of laser-welded thin-plate ship structures based on nominal and structural hot-spot stress approach. *Ships Offshore Struct* 2015;10(1):39–44.
- [61] Murakami Y, Miller KJ. What is fatigue damage? A view point from the observation of low cycle fatigue process. *Int J Fat* 2005;27:991–1005.
- [62] Malitckii E, Remes H, Lehto P, Yagodzinskyy Y, Bossuyt S, Hänninen H. Strain accumulation during microstructurally short fatigue crack propagation in bcc Fe-Cr ferritic stainless steel. *Acta Mater* 2018;144:51–9.
- [63] Lawrence FV, Mattos RJ, Higashida Y, burk JD. Estimating the fatigue crack initiation life of welds. ASTM STP648, Fatigue testing of weldments. Philadelphia 1978:134–58.
- [64] Murakami Y. Metal Fatigue, the Effects of Small Defects and Nonmetallic Inclusions; 2002, Elsevier, Oxford, UK.
- [65] Baumgartner J. Review and considerations on the fatigue assessment of welded joints using reference radii. *Int J Fat* 2017;101:459–68.
- [66] Frank D, Remes H, Romanoff J. On the slope of the fatigue resistance curve for laser stake-welded T-joints. *Fatigue Fract Eng Mater Struct* 2013;36:1336–51.